

INCREMENTAL TRADE-OFF STUDY OF A HYDROGEN FUEL CELL-BASED PROPULSION SYSTEM USING MDAO TECHNIQUES

Roberto DI GIUSEPPE^{1, 2}, Scott DELBECQ¹, Vincent PAUVERT² & Valérie POMMIER-BUDINGER¹

¹Fédération ENAC ISAE-SUPAERO ONERA, Université de Toulouse, France ²Safran Tech - Safran Group, Blagnac, France

Abstract

The aviation sector's carbon footprint reduction strategy has two main components: aircraft energy efficiency improvements and the use of low-carbon alternative fuels. The electrification of aircraft propulsion systems, particularly fuel cell propulsion systems, is one solution being explored that overlaps these two pathways. This paper proposes an incremental trade-off study of a hydrogen fuel cell-based propulsion system using MDAO (Multidisciplinary Design Analysis and Optimization) techniques. The study aims to optimize the design of a fuel cell propulsion system, which includes a fuel cell stack, an electric compressor, a heat exchanger, and an electric motor with integrated power electronics. It examines the interdependencies of these components, their thermal management, and the overall system efficiency and mass. The methodology involves identifying design variables and constraints, understanding the couplings between disciplines, and formulating an efficient optimization problem. The results highlight the need for a system-level study to effectively integrate these components and explore trade-offs in design, considering aspects such as the operating point of the fuel cell stack, thermal efficiency, and system mass.

Keywords: Fuel Cell, Hydrogen, More electric aircraft, MDAO

Nomenclature

```
Compressor
```

```
\pi Compressor pressure ratio [-] c_p Specific heat capacity [-]
```

mass_{cmp} Air compressor mass [kg]

q Compressor mass flow rate $\left[\frac{kg}{s}\right]$

Electric motor

- α_m Magnet opening ratio [-]
- χ Shape factor [-]
- ω Rotational speed of propulsion shaft $\left[\frac{rad}{s}\right]$
- σ_t Tangential component of Maxwell stress tensor [Pa]
- I_s Phase current [A]
- k_f Lamination factor [-]
- k_{w_p} Winding factor [-]

 $mass_{em}$ Electric motor mass [kg]

 N_s Number of winding turns [-]

 U_{ph} Phase voltage in electric motor winding [V]

B Magnetic field [T]

T Mechanical torque on propulsion shaft $[N \cdot m]$

Fuel cell

 $mass_{fc}$ Fuel cell stack mass [kg]

 p_{cath} Air pressure at fuel cell cathode inlet [Pa]

 v_{cell} Single cell voltage [V]

j Current density in fuel cell plates $\left[\frac{A}{m}\right]$

N Number of fuel cell cells [-]

S Fuel cell surface $[m^2]$

Heat exchanger

 α Ratio of fin surface area to the total surface area for heat transfer [-]

b Plate spacing [m]

c Fin pitch [m]

 d_h Hydraulic diameter [m]

L Cold flow length [m]

mass_{hex} Heat exchanger mass [kg]

 t_f Fin thickness [m]

x Fin offset [m]

Inverter

mass_{inv} Power inverter mass [kg]

Cables

mass_{cbl} Cables mass [kg]

 T_{cbl} Cable conductor temperature [${}^{\circ}C$]

 T_{max} Max temperature in cable conductor [°C]

1. Introduction

The growing interest in environmental sustainability pushes academics and industrials to search for disruptive technologies that could reduce the carbon footprint of the aviation sector. For this purpose, the two main technological levers are the improvement of the aircraft's energy efficiency and the use of low-carbon energy carriers [1]. The electrification of aircraft propulsion systems, particularly fuel cell propulsion systems, is one solution being explored that overlaps these two pathways [2].

As fuel cell propulsion systems are still in their infancy, the best system topologies and sizing tradeoffs - in favor of minimizing mass, losses or compactness, and ultimately on-board energy - are not yet known. The interrelations between the fuel cell stack, thermal management system, and electric network require investigation. The fuel cell stack's operating point is determined by the cell's current density and voltage. Maximizing their product for a given stack will increase power density output but increase thermal losses at the same time. Therefore, the design trend for fuel cells suggests that thermal efficiency could be improved by over-sizing the cells[3]. The sizing of the stack has an impact on the voltage of the direct current bus, which in turn affects the sizing of the converter modules and filters, as well as the configuration and size of the motor winding. Furthermore, the operating conditions evolve during the flight in terms of atmospheric characteristics, load and speed requirements. Therefore, the proposed approach must be able to provide a solution that meets the requirements at the multiple given points.

All these considerations lead to the need for a system-level design capable of taking into account the couplings between the disciplines. MDAO (Multidisciplinary Design Analysis and Optimization) has been identified as the most appropriate method to conduct this type of research [4]. In this case, constraints play a crucial role in ensuring that the optimizer does not arrive at impractical or unfeasible solutions. They prevent the selection of unrealistic component shapes or operation points that fall outside the valid range of the models or exceed the technological limits of the components. This study focuses on the formulation of a MDAO problem for the design optimization of a system consisting of a fuel cell stack, an electric compressor for the cathode side of the stack, a heat exchanger, a DC/AC converter and an electric motor for a propulsive load (Fig. 1).

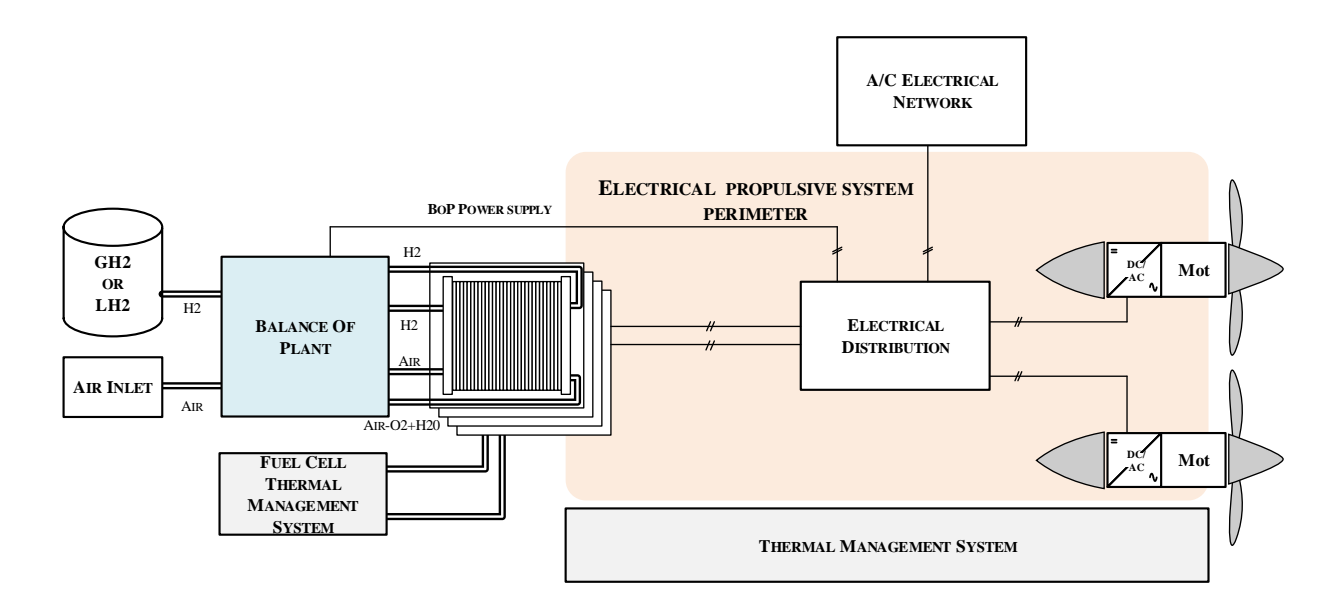


Figure 1 – Overview of the system architecture

First, the models and design variables are identified. Second, the MDAO problem is formulated together with the organization of the coupling variables. Lastly, the results of the optimization are discussed in order to draw conclusions about trade-off points.

2. MDAO for the design optimization of complex systems

MDAO is a methodology to analyse and optimize complex multidisciplinary systems. The central idea of MDAO is to consider the interactions between components using coupled models while simultaneously optimizing the design variables from the various components. In contrast, sequential optimization optimizes one component at a time [5].

MDAO first demonstrated its ability to simultaneously optimize structures and aerodynamics for aircraft design[4]. As stated in [6], MDAO provides a quantitatively supported answer to the "what if" question that arises in the design phase, where specialists want to take advantage of knowing how their decisions might affect other specialists' domains. MDAO tools are now used for the design of complex systems such as aeroplanes [7, 8] and drones [9] but can also be employed for smaller systems or equipment as actuation systems [10] or EMC (Electromagnetic Compatibility) filters [11]. Furthermore, MDAO can support the preliminary design phase since it is supported by visualization methods such as the XDSM diagram [12] that can be useful when iterating on the problem formulation. The XDSM (eXtended Design Structure Matrix) diagram (see Fig. 5) describes the interfaces

and data flows among disciplines of a complex system. The XDSM diagram also contains a numbering system and lines defining the order in which the process is run and the data flow. It provides a compact visualization of the multidisciplinary problems and can be used to reorder the disciplines to reduce feedback loops or support technical discussions between different domain experts.

After studying available open source frameworks [13], the framework chosen in this study to formulate and solve the optimization problem is version 5.1.1 of GEMSEO [14].

3. Models

In this paper, empirical and physics-based models are used for each component of the system (see Tab. 1).

Component	Technology	Model nature	# of inputs/outputs
Fuel cell	LT-PEMFC 1	Empirical / Analytic	6 / 13
BoP ³ compressor	Single stage centrifugal	Empirical / Analytic	4 / 6
Fuel cell heat exchanger	Plate-fin	Analytic	12 / 9
Inverter	2-level 3-phase inverter	Surrogate model	4 / 5
Electric motor	FSCW-PM ²	Analytic	12 / 17
Cables	EWIS standard cable ⁴	Analytic	4/3

Low Temperature Proton-Exchange Membrane Fuel Cell

Table 1 – Component models overview

Fuel cell model

The power source is a low-temperature hydrogen proton-exchange membrane fuel cell (LT-PEMFC). The active surface and the number of cells in a stack are the design variables that determine the shape and mass of the device while the current density is the design variable that fixes the operation point of the stack. A polarization curve links current density and cell voltage. For this study, regression models have been obtained based on available experimental data to model the polarization curve (see Fig 2 where all variables are normalized for confidentiality purposes).

A linear regression model was selected to represent the (j-V) characteristic of the fuel cell. This is because it is well-established that operating the component in the non-linear zone of the curve can lead to its deterioration or problems in controlling low airflow rates. Additionally, non-linear regression models were used to model the impact of cathode air pressure on the polarization curves.

The modelling equation is the following:

$$v_{cell} = a(p_{cathode}) \cdot j + b(p_{cathode}) \tag{1}$$

Where the linearized electrical resistance, a, is interpolated as a function of the pressure at the cathode using a radial basis function (RBF) regressor. Meanwhile, the voltage at zero current, b, is modeled as a function of the pressure using a linear regressor. Hence, by knowing the voltage and current density of the fuel cell, its power output and mass can be computed as a function of the number of cells and active surface area.

$$P_{fc} = v_{cell} \cdot N \cdot j \cdot S \tag{2}$$

$$mass_{fc} = S \cdot (N \cdot c_1 + c_2) \tag{3}$$

Where c_1 , c_2 are two constants that take into account the mass of the cells and the terminal plates. Secondly, the pressure losses in the cathode lines for air are modelled based on the airflow rate, which depends on the current. In this case, polynomial relations have been used.

²Fractional-Slot Concentrated-Winding Permanent Magnet

³Balance of Plant ⁴Electrical wiring interconnection system

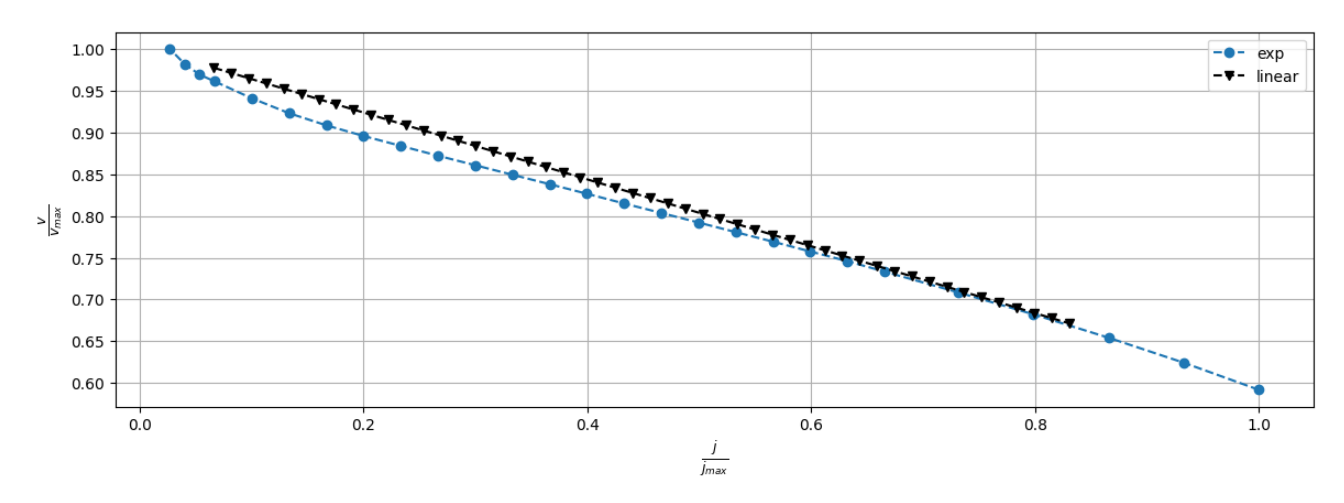


Figure 2 - Comparison between experimental data and the linear models for a given pressure value

Compressor model

A single-stage centrifugal compressor is used to provide the required air mass flow at a given pressure ratio to the fuel cell cathode. Its operating point is derived by interpolation of a reference performance map. As for the design optimization, a reference map is given with a design point (q,π) corresponding to maximum efficiency. The following scaling can be applied:

$$\pi_{map,new} = \pi_{map,ref} \cdot \frac{\pi_{design,new}}{\pi_{design,ref}}$$

$$q_{map,new} = q_{map,ref} \cdot \frac{q_{design,new}}{q_{design,ref}}$$
(4)

The adiabatic efficiency is interpolated in the compressor map. Hence, by knowing the efficiency the outlet temperature is computed so that the power of the mechanical power demanded by the compressor will be:

$$P_{cmp} = q_{corr} \cdot c_p \cdot (T_{out} - T_{atm}) \tag{5}$$

MDAO allows converging to a point inside the map that can be suitably scaled in order to meet the requirements. The selection of the new design point (q,π) must take into account the compressor technology to avoid sizing a component that is technologically unfeasible due to excessively demanding airflow or compression ratio requirements. Moreover, it is critical to carefully account for the various operating conditions under which the compressor will function. Finally, the compressor and its electric motor weights are estimated via empirical law from [7].

Heat exchanger model

An offset strip fin heat exchanger could be an effective technology for this type of system. The extended surface area with a high area-to-volume ratio makes it suitable for applications where compactness is required.

The coolant is a mix of water and ethylene glycol that is cooled by the ambient air. The heat exchanger model employs power-law expressions to determine friction and Colburn factors applicable to a rectangular offset strip fin exchanger [15]. Its design is crucial to consider because of the additional mass on the system and the induced drag which in turn requires extra thrust and consequently more power from the fuel cell stack.

It is important to note that a heat exchanger used in this manner utilizes air as a heat sink, thus its design is strongly dependent on the fluidic properties of air, especially temperature, pressure, and velocity (see Tab.2).

The sizing process, as outlined in [16], computes the volume of the heat exchanger by considering the heat to be dissipated and the Logarithmic Mean Temperature Difference (LMTD), along with the fin efficiency η , the ratio of fin surface area to the total surface area for heat transfer α and the convective heat exchange coefficient h.

Ambient temperature	25°C
Airflow speed	$5\mathrm{ms^{-1}}$
Ambient pressure	101.3 kPa

Table 2 – Sizing conditions for take-off

$$V_T = \frac{Q}{\Delta T_{LM}} \left[\frac{1}{\eta_1 \alpha_1 h_1} + \frac{1}{\eta_2 \alpha_2 h_2} \right] \tag{6}$$

The heat dissipation relies on the fuel cell efficiency, while the LMTD hinges on the inlet and outlet fluid temperatures. The fin efficiency is computed as a function of the convective heat exchange coefficient and geometry, thus dependent on both geometry and fluid properties.

$$\alpha, \eta, h = f(t_f, c, x, b) \tag{7}$$

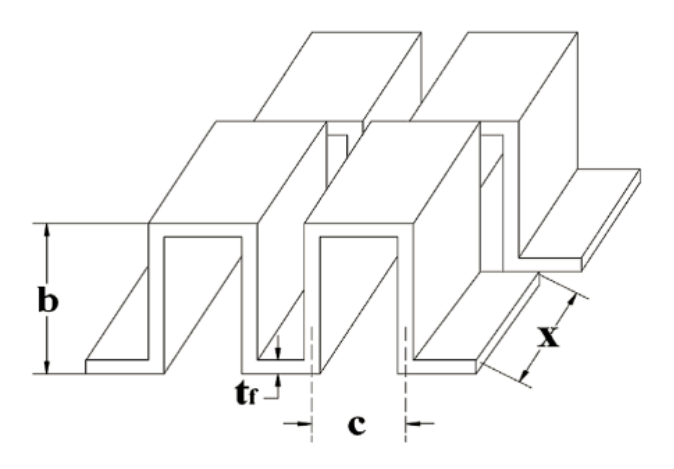


Figure 3 – Fin geometry [16]

In this study, the geometry parameters represented in Fig.3 (the fin thickness t_f and length x, the fin pitch c and the plate spacing b) are kept constants. Indeed, changing these parameters is not straightforward because the components are standardized and the parameters cannot take all the continuous values that would be computed if they were declared as optimization variables. Addressing this type of discrete design problem is recognized as a major challenge [16]. Its consideration would necessitate additional constraints, overburdening the optimizer.

The frontal area of the heat exchanger is the surface exposed to the airflow coming from the external ambient air and it could generate a considerable drag force on the aircraft. It is defined by the conservation of the air mass at the heat exchanger inlet:

$$A_{fr_{cold}} = \dot{m}_{air} \rho v_{air} \tag{8}$$

The cold flow length L is then defined based on the total volume computed in Eq.6:

$$L = \frac{V_T}{A_{freeld}} \tag{9}$$

The cold flow length is a coupled variable that allows also to compute the free flow area $A_{c_{hot}}$ at the inlet of coolant fluid by using α , the hydraulic diameter d_h and the height of the exchanger H:

$$A_{c_{hot}} = \frac{\alpha d_h}{4} HL \tag{10}$$

The implicit system of equations (see Fig.4) is then solved using the Gauss-Seidel method.

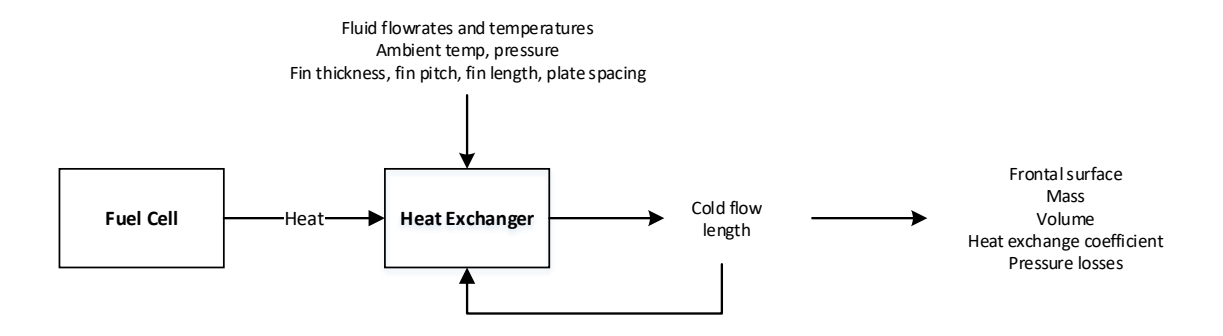


Figure 4 – Schematic of the sizing model for the heat exchanger

Cables model

The sizing process for harnesses takes into account power, DC voltage, altitude, ambient temperature, and the configuration of the bundle with its topology and type of conductors. Derating coefficients based on the harness configuration and environmental conditions are estimated. Additionally, the temperature reached in steady-state operation is determined based on the derated current according to a standard for the installation of wiring used in aerospace vehicles. Aluminum is chosen as the material for the conductors. The length of the cables is also fixed, assuming a nacelle installation for the entire propulsion unit.

Inverter model

A 2-level 3-phase static inverter converts the DC voltage output from the fuel cell to AC voltage for the motor. A surrogate model allows the mass to be estimated. The mass results from the sum of the masses of the different components inside the converter including the semiconductor power modules, the heat sink, and inductive and capacitive filters. The masses of the modules and heat sink are determined via linear regression using data sheets of the modules selected by GT-PowerForge, a third-party software [17]. Meanwhile, the masses of the filters are determined through physics-based analytical equations. Additional mass due to the integration of the component is also considered. In addition to the mass, the output AC current ripple ΔI is computed using Eq. 11, where f_{switch} is the switching frequency fixed to $24 \, kHz$ and L_s is the electric motor phase inductance. The ripple current will be constrained in the optimization problem to be less than 10% of the phase current.

$$\Delta I = \frac{U_{dc}}{6.9 \ f_{switch} \ L_s} \tag{11}$$

Electric motor model

The sizing model of the electric motor is based on an analytical approach that relies on the fundamental physical laws of electric machines. The model integrates variables specific to a Fractional-Slot Concentrated-Windings Permanent Magnet (FSCW-PM) motor [18] and considers a set of geometric variables as inputs, in addition to key requirements such as the torque and the shaft speed. The input variables influencing the design include the stator and rotor dimensions, the fractional slot configuration, the concentrated winding arrangements and the permanent magnet properties. These variables simultaneously impact the electric motor's performance and its interaction with the fuel cell within the propulsion system.

Firstly, the winding layout in the stator is defined so that the fundamental winding factor k_{w_p} is fixed at the beginning.

After that, it is possible to compute the tangential pressure in the airgap σ_t by knowing the linear current density A_{rms} and the airgap magnetic induction B_{δ_1} :

$$\sigma_t = \frac{A_{rms} \cdot B_{\delta_1}}{\sqrt{2}} \cdot cos(\delta) \cdot k_{w_p} \tag{12}$$

It was assumed that the electric motor would be cooled by oil in order to determine the bounds for the current density. Once the tangential pressure is known, the torque T required allows the rotor volume V_r to be determined:

$$V_r = \frac{T}{2 \cdot \sigma_t} \tag{13}$$

Hence, the choice of the shape factor χ fixes the airgap diameter D_{δ} :

$$D_{\delta} = \sqrt[3]{\frac{4V_r}{\chi \cdot \pi}} \tag{14}$$

Once the diameter has been fixed, the height of the stator h_{cs} , the rotor yokes h_{cr} , and the width of the stator teeth b_d are defined as functions of the magnetic induction values in their respective zones:

$$b_d, h_{cs}, h_{cr} = f(\tau_d, B_{\delta}, k_f, B_x, \alpha_m) \tag{15}$$

Where B_x indicates the magnetic induction in the respective zone.

Then, the height of the magnets is determined by using Ampère's circuital law. After establishing the geometry, the inductance of the electric motor can be calculated. It is therefore possible to calculate the phase voltage across a single turn of the stator winding U_{ph_1} . The total voltage U_{ph} is calculated as follows:

$$U_{ph} = N_s \cdot U_{ph_1} \tag{16}$$

In the formulation problem proposed here, the number of turns is chosen as the variable that allows for the adaptation of the electric motor voltage to the stack voltage output (see Fig.5). The number of slots in the motor is selected based on a study conducted to analyze the impact of this parameter on the machine inductance and subsequently on the current ripple. The phase inductance L_s is computed as product of total permeance Λ_{tot} and number of turns:

$$L_s = \Lambda_{tot}(Q_s, \dots) \cdot N_s^2 \tag{17}$$

Where Q_s is the number of slots. Therefore, the optimal compromise value between a tolerable current ripple (see Eq.11) and mass has been identified. Once the number of turns is known, the phase inductance and resistance, along with the motor size constant and back EMF constant can be calculated. Consequently, the power factor can be deduced, along with the losses.

4. Problem formulation

The paper then proposes to analyze and optimize the system incrementally, adding one discipline at a time, to end up with the global system, as shown in the XDSM diagram (see Fig. 5). Although the final result is more relevant to the propulsion system analysis, solving intermediate optimization problems has allowed an understanding of which variables are coupled between the models of different components, what are the suboptimal designs, and how adding other components influences these interdependencies.

A solver is used to manage the main coupling variables:

- U_{dc} , U_{ph} , the direct current bus and phase voltages,
- *P_{cmp}*, the power of the compressor demanded by the fuel cell,
- L, the cold flow length of the heat exchanger, as explained previously in Fig.4

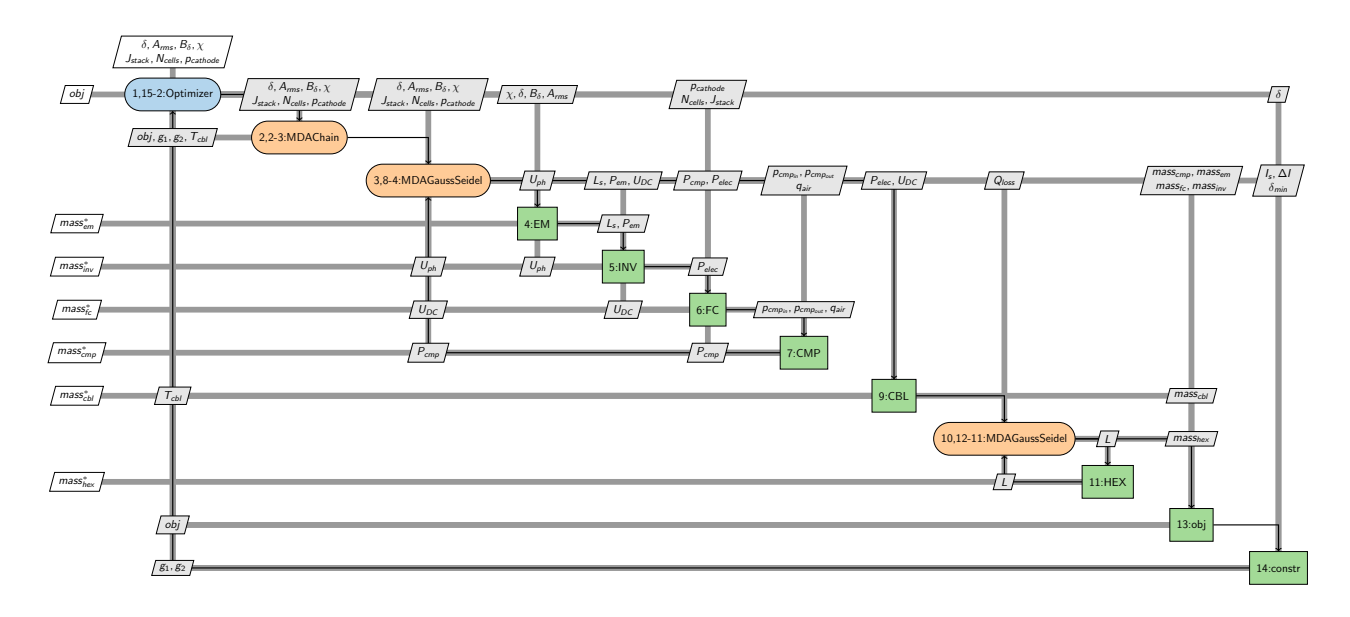


Figure 5 – XDSM diagram [12] representing the optimization problem architecture for the global system

The optimization problem (Eq. 18) is solved using the gradient descent algorithm SLSQP because it can handle both the equality and inequality constraints, and the derivatives are approximated using finite differences.

$$\begin{aligned} & \min_{x \in X} \quad f(x) = \sum_{j=1}^{n} mass_{j}(x) \\ & \text{w.r.t.} \quad j_{fc}, \, N, \, p_{cath}, \, \delta, \, A_{rms}, \, B_{\delta}, \, \chi \\ & \text{s.t.} \quad \delta \geq \delta_{min}(A_{rms}, \, B_{\delta}, \, \chi), \\ & \frac{\Delta I}{I_{s}} \leq ripple_{max}, \\ & T_{cbl} \leq T_{max} \end{aligned} \tag{18}$$

- j_{fc} , current density in fuel cell stack
- N, number of cells in a stack
- p_{cath}, air pressure at cathode inlet in the fuel cell stack
- δ , airgap in the electric motor
- A_{rms}, linear current density in electric motor
- B_{δ} , magnetic field in the airgap
- χ , shape factor of the electric motor

4.1 Couplings organization

Once the models are established, there are several ways to integrate them into an optimization problem-solving architecture. In this study, the MDF formulation is selected to reduce the load on the optimizer and have a consistent design at each optimizer iteration. The coupling variables are the compressor power between the compressor and the fuel cell, the DC bus voltage between the fuel cell and the inverter, and the phase AC voltage between the inverter and the electric motor (see Fig. 5).

In order to determine the phase voltage and, ultimately, the number of turns in the motor winding, the DC bus voltage is selected as a coupling variable between the fuel cell and the inverter (see Eq.16). The coupling is necessary because the surface of the stack cannot be determined without knowing the electric power supplied by the motor.

Similarly, the power required by the compressor depends on the current generated by the fuel cell stack. Once the compressor power is known, the fuel cell stack's surface is computed in turn. Again, this is an algebraic loop that is solved numerically.

5. Results and discussion

The MDAO problem is well posed, and the study presented here for the most demanding flight phase, namely takeoff, can be extended to consider other flight phases in a larger multipoint optimization problem. The optimization problem presented in Eq. 18 was divided into three subsequent steps.

The first step in the study was to solve the optimization problem of the fuel cell with the air compressor. In a fuel cell, the surface power density per cell increases with increasing cathodic air pressure [19]. The use of a compressor is necessary to compress air to the appropriate pressure for the proper operation of the fuel cell. However, the beneficial effect of increased pressure for the fuel cell entails a heavier compressor, due to the higher compression ratio it must deliver. Therefore, the solution returns the pair (p_{cath}, j_{max}) beyond which the decrease in stack mass is less than the increase in compressor mass. Meanwhile, the number of cells in the solution corresponds to the upper maximum limit.

The second step was to include the heat exchanger sizing in the same optimization problem to assess to what point it is relevant to oversize the fuel cell stack at the expense of its thermal efficiency. As emphasized in section 3, no optimization variable was chosen for the heat exchanger since it was desired to utilize an existing adaptable component by overlaying plates in the height direction or increasing the length of cold airflow. The heat exchanger shifts the equilibrium point (p_{cath}, j) because the efficiency of the stack varies depending on this point. Decreasing the current density in the stack is beneficial because it improves efficiency. Furthermore, the voltage increase consequently reduces the current that the stack must deliver, and the compressor can be sized to deliver a smaller quantity of air at higher pressure (see Fig. 7). These considerations are valid for sizing during takeoff and sensitive to flight conditions because ambient pressure and temperature have an antagonistic effect on the compressor and heat exchanger compared to the increase in mass. Indeed, a heat exchanger sized at cruise altitude would benefit from lower temperatures and higher airflow passing through its channels.

The final step was to include the sizing models related to the electric motor, the inverter and the cables to the optimization problem to analyze the impact on the optimal bus DC voltage. The objective is to study all the sizing problems defined so far in the same formulation of the multidisciplinary problem. In the sizing procedure followed (see Fig. 5), the DC bus voltage is determined by the fuel cell by choosing the number of cells and the operating point on its polarization curve. Consequently, the phase voltage in the electric motor is set through the inverter, and therefore, the number of turns in each coil is fixed through the eq. 16. As for the optimization variables, the electric motor with the minimum mass is found to have the maximum linear current density in the winding and the lowest shape factor. This results in a motor with a very large diameter compared to its length in order to maximize the mechanical couple with a lower electromagnetic force (Fig. 6).

As for the inverter, the influence of voltage is seen in its mass, which decreases with increasing voltage. At higher voltages, filters, heat dissipation plates, and semiconductor modules become lighter.

Another important aspect to consider in the sizing of this propulsion system concerns the voltage variation between the take-off phase, for which the system is sized, and the idle phase. The approach followed in this case was to fix the maximum number of fuel cell stacks based on the minimum current density allowed on the polarization curve (resulting in a maximum cell voltage) and the maximum idle voltage allowed on the DC bus (see Eq.19). The minimum current density in the fuel cell stack is due to the humidity management of the membrane when the reactants flow rate is low because the component would be damaged if $j \leq j_{min}$, while $V_{idle_{max}}$ is fixed by the electrical insulation constraints.

$$N_{cells_{max}} = \frac{V_{idle_{max}}}{v_{cell_{max}}} \tag{19}$$

The fuel cell stack and the heat exchanger account for the most of the mass because of their low power density (see last column in Fig. 9). It must be noted that the fuel cell counts only for the mass of the stack without considering the integration, while the masses of the other components also consider the integration parts. Furthermore, the optimization of the core geometry of the heat exchanger remains to be evaluated. Finally, it can be observed that the inverter and the compressor

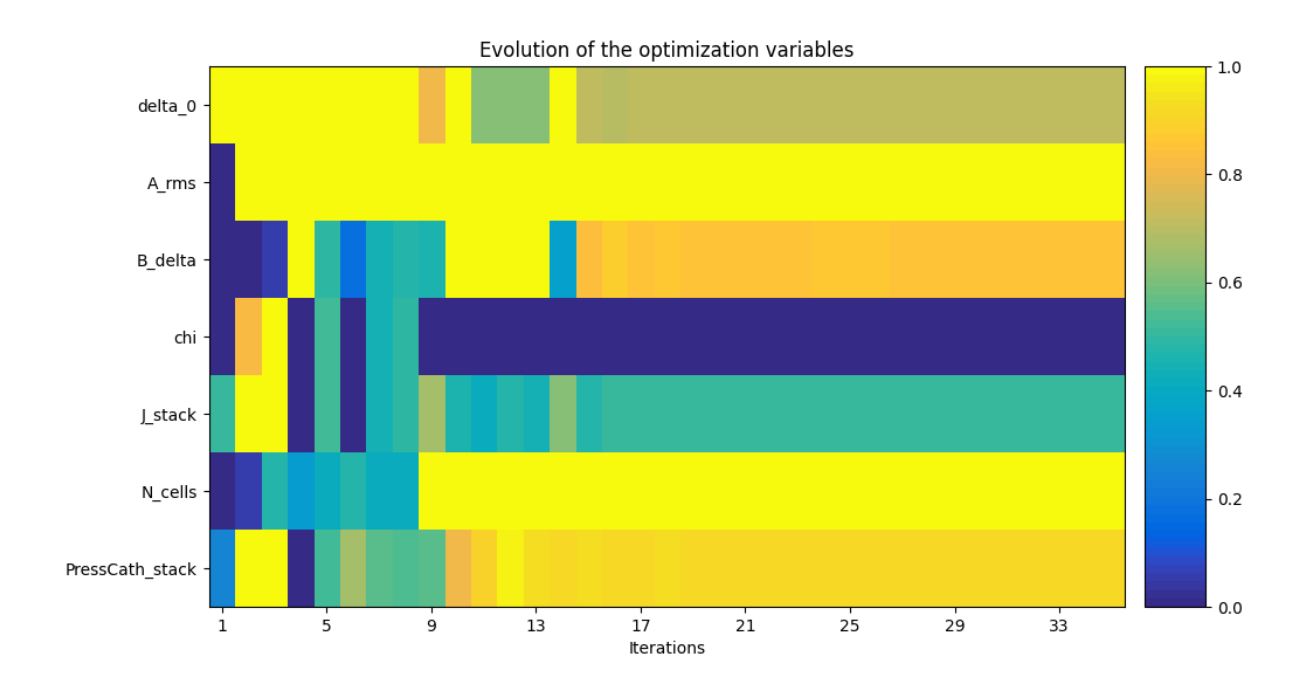


Figure 6 – Evolution of optimization variables

have more or less the same weight. However, the power required from the stack to operate the compressor is higher than the power losses of the inverter.

Fig. 7 gives the evolution of the fuel-cell sizing point on the polarization curve. The sizing point strongly depends on the heat exchanger. As the operating voltage of the fuel cell stack increases, the efficiency of the fuel cell stack also increases, and consequently, less heat needs to be dissipated, resulting in a decrease in the mass of the heat exchanger. Conversely, when a fuel cell stack's operating voltage rises, its specific power falls. For a given power need, this causes the mass of the fuel cell to grow. Thus the figure shows that it is preferable to use a heavier stack at a lower power density to benefit from higher efficiency. Similarly, increasing the cathodic pressure requires a more massive compressor on one hand, but allows exploiting the stack with higher efficiency.

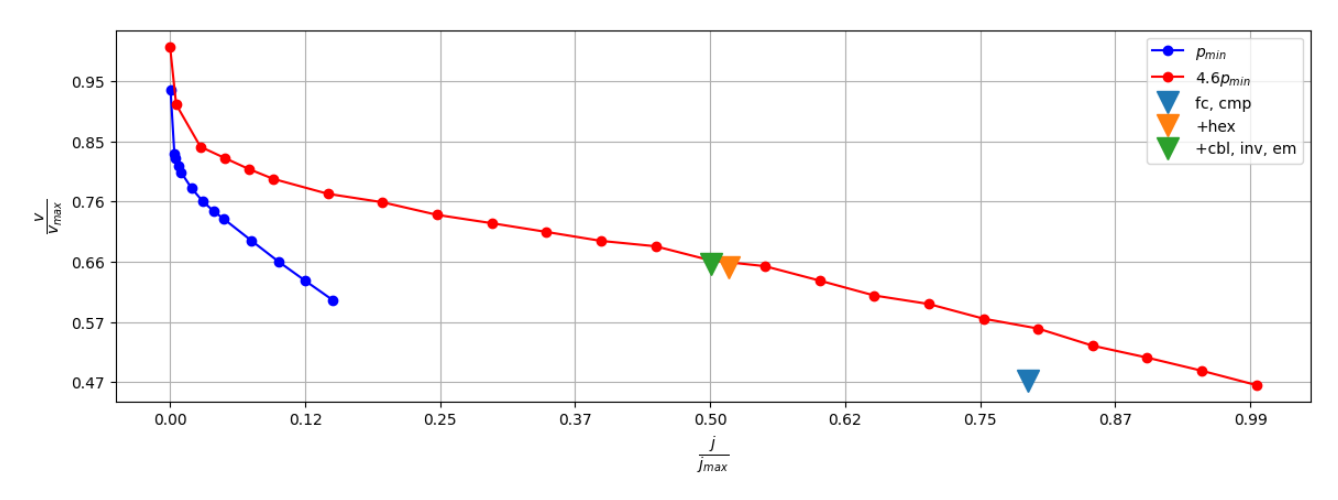


Figure 7 – Evolution of the fuel-cell sizing point

In order to minimize mass, the design of the components requires high current densities, which results in a loss of efficiency due to increased dissipated heat. Fig. 8 shows the variations in mass and efficiency on the plotted Pareto front, and Fig. 9 shows the reduction in system mass at the expense of the thermal dissipation system mass. At the same time, lower efficiency would also mean higher hydrogen consumption, so the advantageous mass reduction of the fuel cell stack and electric

motor could be less than the mass increase of the hydrogen storage system.

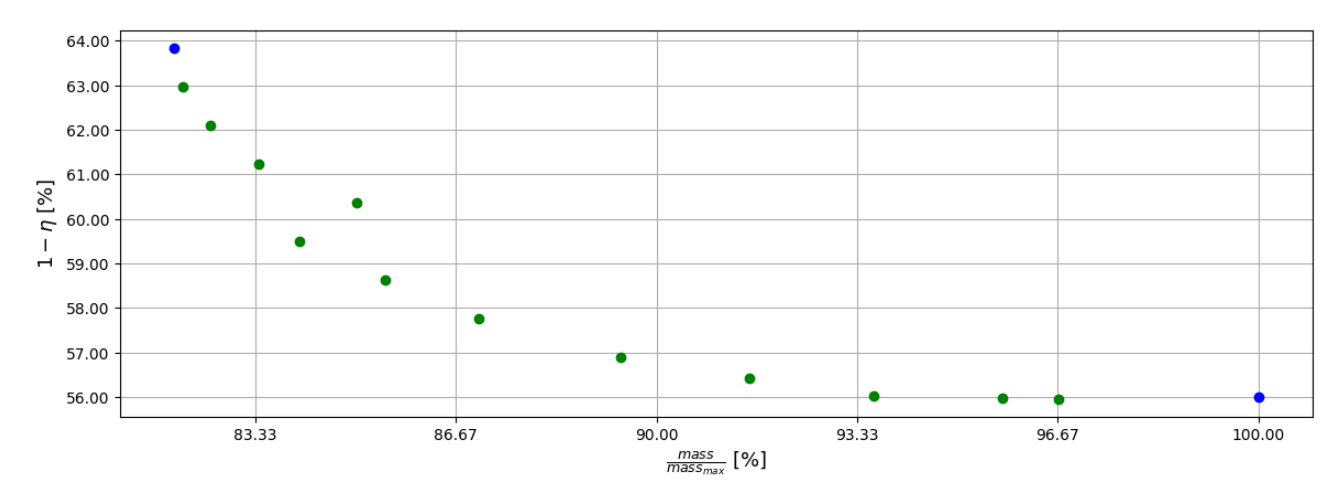


Figure 8 – Pareto frontier between mass and losses

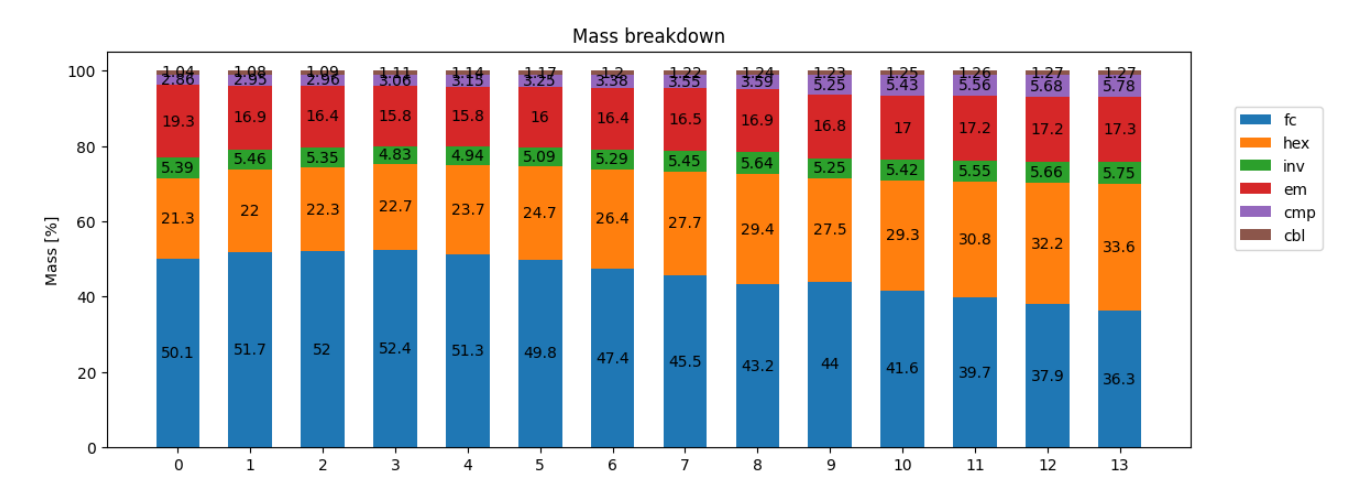


Figure 9 – Preliminary estimation of mass breakdown for points in Pareto front (decreasing mass)¹

6. Conclusions

Several new tools are available to designers for conceiving complex engineering systems. In a design task such as the one illustrated in this study, the accuracy of the result depends on both the optimization algorithm and the formulation of the optimization problem, as well as on the fidelity of the models used. The incremental approach employed in this study has enabled the integration of models in a step-wise manner, a methodology that aligns with the typical operations of industrial design departments, where less detailed models are initially used to identify first-order trends, followed by refinement, if necessary.

The MDAO framework has aided in the exchange of data between models of heterogeneous nature, and in the resolution of the set of implicit equations. In particular, the governing equations in the models have been developed in order to identify the optimal choice of coupling variables that the solver must process. This choice is driven by the knowledge of the models and by the degree of detail required for the preliminary design.

The results show that the sizing point of the fuel cell stack is strongly dependent on its auxiliary systems, which includes the thermal management system and the compressor. In addition, the impact of the stack on the electric-mechanical conversion system has been considered in the preliminary design phase to address constraints that would otherwise result in an increase in mass and volume of the components if considered separately.

¹The mass of the fuel cell stack considers only active parts.

The optimization problem for the case of study has been well posed, the main design variables have been identified along with the constraints and a suitable algorithm. The most demanding flight phase, the take-off, has been considered for sizing and the problem structure has been carefully formulated to prepare the ground for a larger study that will take into account other flight conditions at the same time in the optimization problem. The objective of this further study is to ascertain the extent to which conclusions derived from take-off phase optimization remain valid in a multi-point optimization scenario, and if different flight conditions exert a significant influence on the sizing trend.

Copyright Statement

The authors confirm that they, and/or their company or organization, hold copyright on all of the original material included in this paper. The authors also confirm that they have obtained permission, from the copyright holder of any third party material included in this paper, to publish it as part of their paper. The authors confirm that they give permission, or have obtained permission from the copyright holder of this paper, for the publication and distribution of this paper as part of the ICAS proceedings or as individual off-prints from the proceedings.

References

- [1] S Delbecq, J Fontane, N Gourdain, T Planès, and F Simatos. Sustainable aviation in the context of the paris agreement: A review of prospective scenarios and their technological mitigation levers. *Progress in Aerospace Sciences*, 141:100920, 2023.
- [2] Eytan J. Adler and Joaquim R.R.A. Martins. Hydrogen-powered aircraft: Fundamental concepts, key technologies, and environmental impacts. *Progress in Aerospace Sciences*, 141:100922, 2023. Special Issue on Green Aviation.
- [3] Thomas Kadyk, Christopher Winnefeld, Richard Hanke-Rauschenbach, and Ulrike Krewer. Analysis and design of fuel cell systems for aviation. *Energies*, 11(2), 2018.
- [4] J. Sobieszczanski-Sobieski and R.T. Haftka. Multidisciplinary aerospace design optimization: survey of recent developments. *Structural Optimization*, 14:1–23, 1997.
- [5] Joaquim R. R. A. Martins and S. Andrew Ning. *Engineering design optimization*. Cambridge University Press, Cambridge; New York, NY, 2021.
- [6] Jaroslaw Sobieszczanski-Sobieski. Sensitivity analysis and multidisciplinary optimization for aircraftdesign recent advances and results. *Journal of Aircraft*, 27(12):993–1001, December 1990.
- [7] Vincenzo Palladino, Arnaud Jordan, Nathalie Bartoli, Peter Schmollgruber, Valerie Pommier-Budinger, and Emmanuel Benard. Preliminary studies of a regional aircraft with hydrogen-based hybrid propulsion. In *AIAA AVIATION 2021 FORUM*, VIRTUAL EVENT, 2021. American Institute of Aeronautics and Astronautics.
- [8] Ruben Perez, Hugh Liu, and Kamran Behdinan. Evaluation of multidisciplinary optimization approaches for aircraft conceptual design. In *10th AIAA/ISSMO Multidisciplinary Analysis and Optimization Conference*. American Institute of Aeronautics and Astronautics, August 2004.
- [9] S. Delbecq, M. Budinger, A. Ochotorena, A. Reysset, and F. Defay. Efficient sizing and optimization of multirotor drones based on scaling laws and similarity models. *Aerospace Science and Technology*, 102, July 2020.
- [10] Scott Delbecq, Marc Budinger, Dimitri Leray, Jérôme Piaton, and Benjamin Dagusé. Optimization of primary flight control actuation system using parametric sizing models of actuators, power electronics and structural analysis. pages 132–138, Toulouse, France, 2018.
- [11] Arthur Piat, Hans H. Sathler, Francois Gallard, and Bernardo Cougo. A multidisciplinary design optimization approach for emc filters design for more electric aircraft applications. In 2021 23rd European Conference on Power Electronics and Applications (EPE'21 ECCE Europe), pages P.1–P.10, Ghent, Belgium, September 2021. IEEE.
- [12] Andrew B. Lambe and Joaquim R. R. A. Martins. Extensions to the design structure matrix for the description of multidisciplinary design, analysis, and optimization processes. *Structural and Multidisciplinary Optimization*, 46(2):273–284, 2012.
- [13] R. di Giuseppe, S. Delbecq, V. Budinger, and V. Pauvert. An exploratroy study of open-soruce frameworks for MDAO. In *II ECCOMAS Thematic Conference on Multidisciplinary Design Optimization of Aerospace Systems*, pages 478–494, Lisbon, Portugal, July 2023.
- [14] F. Gallard, C. Vanaret, D. Guénot, V. Gachelin, R. Lafage, B. Pauwels, P.-J. Barjhoux, and A. Gazaix.

Incremental trade-off study of a hydrogen fuel cell-based propulsion system using MDAO techniques

- Gems: A python library for automation of multidisciplinary design optimization process generation. In 2018 AIAA/ASCE/AHS/ASC Structures, Structural Dynamics, and Materials Conference, 2018.
- [15] Raj M. Manglik and Arthur E. Bergles. Heat transfer and pressure drop correlations for the rectangular offset strip fin compact heat exchanger. *Experimental Thermal and Fluid Science*, 10(2):171–180, 1995.
- [16] Guo Kunpeng. *Optimisation of Plate/Plate-Fin Heat Exchanger Design*. PhD thesis, The University of Manchester, 2015.
- [17] Gamma Technologies. Gt-powerforge. https://www.gtisoft.com/gt-powerforge-2/, 2024. Power converter design software.
- [18] Florence Meier. Permanent-magnet synchronous machines with non-overlapping concentrated windings for low-speed direct-drive applications. 2008.
- [19] James Larminie and Andrew Dicks. Fuel Cell Systems Explained. Wiley, 1 edition, February 2003.